Recurrent energization of plasma in the midnight-to-dawn quadrant of Saturn's magnetosphere, and its relationship to auroral UV and radio emissions

D.G. Mitchell [a,*], S.M. Krimigis [a], C. Paranicas [a], P.C. Brandt [a], J.F. Carbary [a], E.C. Roelof [a], W.S. Kurth [b], D.A. Gurnett [b], J.T. Clarke [c], J.D. Nichols [d], J.-C. Gérard [e], D.C. Grodent [e], M.K. Dougherty [f], W.R. Pryor [g]

[a] *Johns Hopkins University Applied Physics Laboratory, MP3 E-132, 11100 Johns Hopkins Road, Laurel, MD 21042, USA*
[b] *Department of Physics and Astronomy, University of Iowa, Iowa City, IA, USA*
[c] *Center for Space Physics Boston University, Boston, USA*
[d] *Department of Physics and Astronomy, University of Leicester, Leicester, UK*
[e] *Laboratoire de Physique Atmosphérique et Planétaire Université de Liège, Belgium*
[f] *Blackett Laboratory, Imperial College, London, UK*
[g] *Central Arizona College, Coolidge, AZ, USA*

ABSTRACT

We demonstrate that under some magnetospheric conditions protons and oxygen ions are accelerated once per Saturn magnetosphere rotation, at a preferred local time between midnight and dawn. Although enhancements in energetic neutral atom (ENA) emission may in general occur at any local time and at any time in a Saturn rotation, those enhancements that exhibit a recurrence at a period very close to Saturn's rotation period usually recur in the same magnetospheric location. We suggest that these events result from current sheet acceleration in the 15–20 Rs range, probably associated with reconnection and plasmoid formation in Saturn's magnetotail. Simultaneous auroral observations by the Hubble Space Telescope (HST) and the Cassini Ultraviolet Imaging Spectrometer (UVIS) suggest a close correlation between these dynamical magnetospheric events and dawn-side transient auroral brightenings. Likewise, many of the recurrent ENA enhancements coincide closely with bursts of Saturn kilometric radiation, again pointing to possible linkage with high latitude auroral processes. We argue that the rotating azimuthal asymmetry of the ring current pressure revealed in the ENA images creates an associated rotating field aligned current system linking to the ionosphere and driving the correlated auroral processes.

© 2009 Elsevier Ltd. All rights reserved.

1. Introduction

Many measurements of particles and fields in Saturn's magnetosphere (e.g., Kurth et al., 2008; Giampieri et al., 2006; Carbary et al., 2007a) exhibit modulation at a frequency close to that established by the observed modulation of Saturn kilometric radiation (SKR), which has been used to establish the Saturn Longitude System 3 (SLS3, Kurth et al., 2008). Energetic particles in the magnetotail are enhanced approximately once per SLS3 rotation, and energetic neutral atom emission bright spots recur with a period very close to that of the SLS3 period (Paranicas et al., 2005; Carbary et al., 2007b).

Although such periodicity in the energetic particle data is well established, it has not been determined whether there is a preferred local time for the energization of the particles, and if so, where. Because the spacecraft is constantly moving in local time and radius, spending much of its time outside the rotating portion of the magnetosphere and even less in the magnetic equatorial part of that rotating portion where the in situ particle intensities typically peak, pinning down the location of the onset of these events using in situ data is difficult at best. Energetic neutral atom (ENA) imaging by the ion and neutral camera (INCA), a sensor of the magnetospheric imaging instrument (MIMI) on the Cassini spacecraft, permits the remote detection and location of global scale ion acceleration events (Krimigis et al., 2004). In this paper we will show that the initiation of these recurrent acceleration events usually takes place in the midnight to dawn quadrant at radial distances of approximately 15–20 Rs (although they quickly spread to affect a region as close to Saturn as 7 Rs). We show evidence consistent with the interpretation that these events are associated with reconnection.

* Corresponding author. Tel.: +1 443 778 5981; fax: +1 443 778 0386.
E-mail address: don.mitchell@jhuapl.edu (D.G. Mitchell).

Energetic neutral atom emissions imaged by the MIMI INCA sensor have been used in several publications to investigate the rotational modulation of energetic ion enhancements in Saturn's magnetosphere (Krimigis et al., .2005; Paranicas et al., 2005; Carbary et al, 2007b) and to establish the instantaneous and long term locus of the energetic protons and oxygen ions in Saturn's ring current (Krimigis et al., 2007; Carbary et al., 2008b; Brandt et al., 2008). These studies have shown that Saturn's ring current is rarely symmetric (Krimigis et al., 2007; Carbary et al., 2008b), and that the energetic neutral atom enhancements produced as the asymmetric ring current charge exchanges with a roughly symmetric cold neutral gas cloud (Jurac and Richardson, 2005; Shemansky and Hall, 1992) are modulated at approximately the SLS3 period (Paranicas et al., 2005; Carbary et al., 2008a).

Carbary et al. (2008a) further determined that modulation of energetic oxygen ENA is far more regular in its period than is modulation of energetic hydrogen ENA. Paranicas et al. (2005) showed that the modulation exhibited during a particularly stable interval from day 351–358, 2004 could be explained by a combination of a symmetric steady state ring current ENA source located near 10 Rs, superposed with a rigidly corotating point source at 8 (hydrogen) to 9 (oxygen) Rs. The modulation is produced as the point source alternately moves toward and away from the observer, brightening and dimming through the combined effects of a R^{-2} dependence and the Compton-Getting effect. As pointed out by those authors, the situation is more complex—a point source is an oversimplification, and the steady loss of ions through the charge exchange process demands an on-going replacement process; otherwise, the ENA intensities would have decreased over the seven-day interval, whereas their small observed decrease can all be attributed to R^{-2} dependence as the spacecraft moved farther from Saturn.

Left unanswered in those papers are the questions of where and how the ions are being energized to maintain their average intensity, and how the rotation modulation can at the same time be maintained very close to the SLS3 period. The latter behavior is even more puzzling when contrasted with in situ measurements of the plasma flow in the middle and outer magnetosphere (Kane et al., 2008; Mauk et al. 2005) that reveal velocities typically at a fraction of rigid corotation (the term we use to describe an azimuthal velocity sufficient to match the SLS3 period at any given radius).

Mauk et al. (2005), Paranicas et al. (2007), and Brandt et al. (2008) used the gradient and curvature drift of energetic ions and electrons in the inner to middle magnetosphere (6–12 Rs) to determine the age of energy-dispersed energetic particle injections. As a freshly injected population of energetic particles corotates about the planet in the corotation electric field, an additional azimuthal drift controls their loci as a function of time, causing energetic ions to super-corotate ahead of the cold plasma, and energetic electrons to drift against corotation, slowing their azimuthal guiding center velocity. This drift also affects the drift velocities of the ions that are converted to ENA and imaged by INCA. Therefore, the Compton-Getting induced ENA modulation caused by a combination of azimuthal asymmetry, viewing geometry and plasma velocity relative to the observer should also be ordered in energy according to the age of the particle heating event, a characteristic we make use of in the following analysis.

2. Observations

2.1. Energy dispersion of corotating oxygen ENA events

This paper uses two qualitatively different types of ENA observations to explore the question as to where, if anywhere, in local time the corotating ENA enhancements begin and/or are rejuvenated. The first type of observation is conducted from low latitude, such that the ring current is imaged edge-on, and the rotating enhancements tend to maximize as the corotation vector moves the source energetic ion population toward the spacecraft (see Fig. 1). The second type of observation is from high latitude, where the Compton Getting effects are minimized, and where the local time location of an ENA enhancement can be observed directly.

Since the Carbary et al. (2008a) study found that the periodicity was more clearly expressed in neutral oxygen emissions than in hydrogen, and because oxygen intensities at a given energy are more strongly influenced by the Compton-Getting effect than are hydrogen intensities, we restrict our analysis to the edge-on observations of energetic neutral oxygen. Fig. 2 shows whole image integrated ENA intensities for oxygen for the time period studied by Paranicas et al. (2005).

The peaks (and valleys) in the ENA intensity do not occur at the same time for all energies; rather, the peak intensity at the lowest energy lags the peak at highest energy by approximately half of the common modulation period for all ion energies, the lag decreasing with increasing energy. The modulation is consistent with a localized population of increased energetic ion intensity corotating with the plasma, while also gradient and curvature drifting in the same direction as the corotating plasma (Paranicas et al., 2005). The lower energy ions drift more slowly than those at higher energy, and so lag behind the latter, as illustrated conceptually in Fig. 1. By modeling the drift period in a dipole field, we can get a quantitative estimate of the location and time of creation of the rotating ion enhancement (Fig. 3). In this simple simulation, we calculate the time (in hours) it takes for an ion to move from a hypothetical emission local time to a local time 270° from that emission local time, measured in the direction of corotation. The green symbols track the time required for 90° pitch angle ions with a range of energies between 50 and 250 keV to travel 270°, for four different L-shells, namely $L = 8$, $L = 9$,
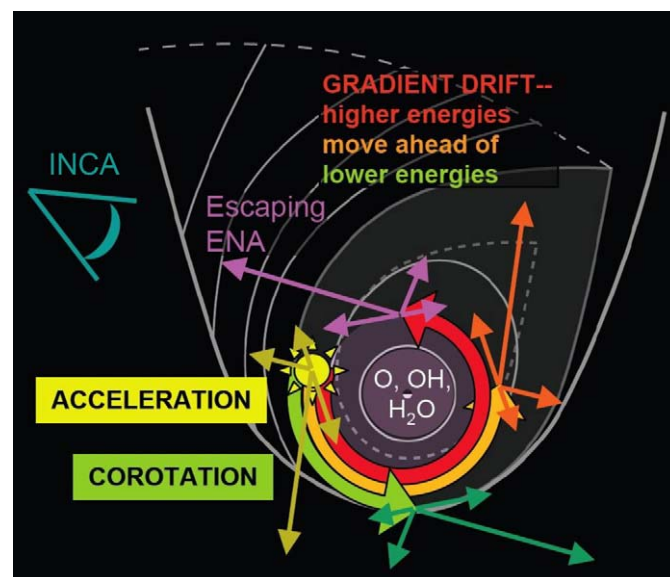

Fig. 1. Following an acceleration event (depicted here as the yellow burst near dawn; the sun is down in this figure) heated particles corotate along with the cold plasma. Some time later, low energy ions have corotated to noon, intermediate energy ions to dusk, and the highest energy ions to midnight. As the Compton-Getting effect results in higher intensities in the direction of the bulk velocity, ENA emission seen by INCA in the pre-dawn sector maximizes as the hot population approaches midnight. Since high energy ions reach midnight before low energy ions, the observed peak intensity at high energies precedes the observed peak at low energies.
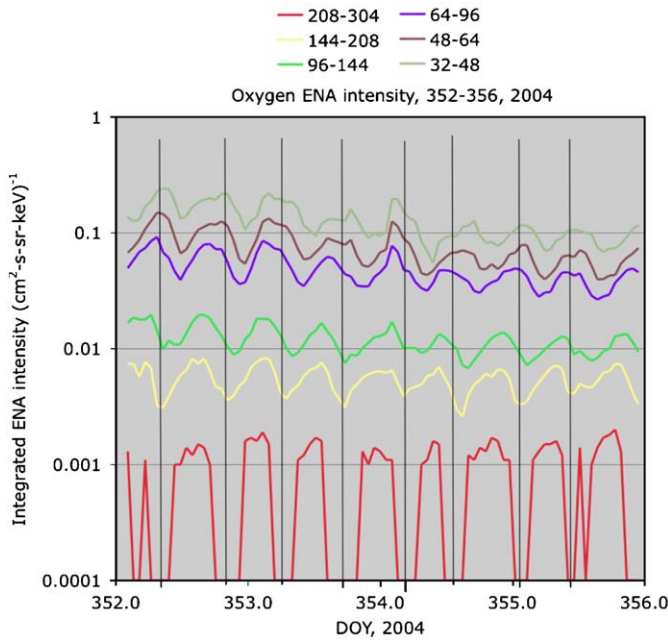
Fig. 2. Intensity of oxygen ENA emission with energies from ~40 to ~250 keV (see legend) over 4 days in late 2004, viewed from 0400 to 0540 LT, −5° latitude, radial distance changing from 20 to 40 Rs over the time period.
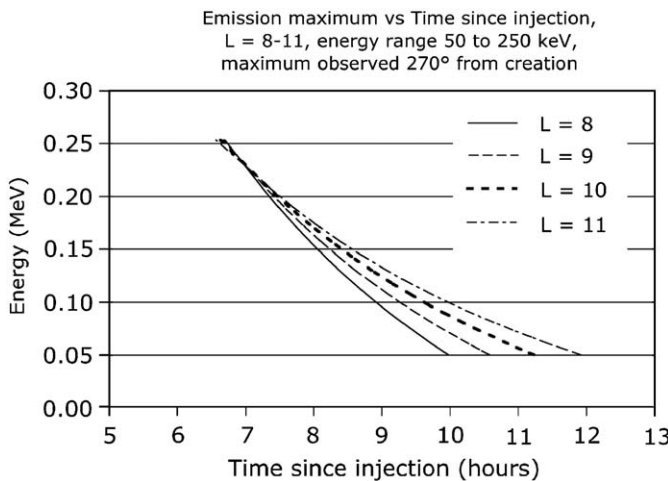

Fig. 3. Example of a parametric model of ion drift in a Saturn dipole field consistent with the data shown in Fig. 2. The four families of points show the time for a range of energies between 50 and 250 keV to convect and drift 270° along four different L shells (8, 9, 10, and 11). This run restricted the particle pitch angles to 90°, so the differences in drift relative to the corotational convection are attributable to gradient-B drift. The convective term uses the corotation speed as a function of L shell derived by Mauk et al. (2005).

$L = 10$, and $L = 11$. At the highest energies, the ions at all L shells move through 270° in about 7 hours, while those at the lowest energies take from 10 to 12.5 hours, depending on L shell (in a dipole field, gradient drifts are faster at large L; this is offset by the dependence of the plasma convection velocity on radial distance– for this simulation, the velocity curve derived by Mauk et al. (2005) was used). For the lowest energy ions, the longest transit times are for $L = 11$, while the shortest are for $L = 8$. At the highest ion energies, the reverse is true, as the gradient drift speed increase with L is slightly greater than the reduction in convective velocity with L. The two effects are essentially matched at about 230 keV ion energy. What this means is that if an observer were to

detect a population of ions (or its associated ENA enhancement) that had traveled through 270° from its point of acceleration, they would detect the high energy (250 keV) ions first, and 3–5.5 hours later they would detect the lowest energy (50 keV) ions. The actual delay would depend on the L-shell. Over the range covered by Fig. 3 ($8 \leqslant L_{dipole} \leqslant 11$), the magnetic field may significantly depart from a dipole (e.g., Bunce et al., 2008). Such deviations (decreased radius of curvature, reduced field magnitude, increased gradient in the region of transition from dipole to stretched field) generally make the results in Fig. 3 a lower limit to the actual case.

The data in Fig. 2 are consistent with the model results shown in Fig. 3, and imply that the creation of the hot ion population took place approximately 270° from where the intensity peak for each energy is observed. By "approximately", we mean that given the inaccuracies in establishing just which L-shell the maximum intensity is on, and to what degree non-dipolar field configuration modifies the drift rates modeled in Fig. 3, the observed ~5.5 hour dispersion could translate to anywhere from about 250° to 330° according to the strict model, but given the likelihood of non-dipolar field, we have suggested a centroid of about 270° rather than 290°. Since the spacecraft is located between 0400 and 0540 during the observation, the intensity maximum should be (and is—see Paranicas et al., 2005) located a little pre-midnight, where the corotation convection velocity vector is roughly toward the Cassini spacecraft. Moving backward in rotation 270° from that location, the implied creation location for these particles is slightly pre-dawn, essentially the same local time as the spacecraft for this event. This example indicates how a dispersion time can be inferred from INCA neutral atom signatures.

We systematically surveyed all of the data for which clear-cut rotation modulation was observed in the oxygen ENA intensities, and made an estimate of the dispersion time observed in each event using the drift method outlined above. With viewing geometry restricted to vantage points close to the equatorial plane, the ENA emission is dominated by 90° pitch angle particles near the equatorial plane, making the modeling of gradient drift only appropriate. The results are summarized in Fig. 4. The dispersion clearly shows local time dependence, with a minimum in the late morning hours and a maximum in the early morning hours. The transition from maximum to minimum across the dawn quadrant is fuzzy, probably because events which are created near dawn may exhibit peak intensity either just as they are created, or after 270°–360° of rotation. They may also present two peaks, which may smear together and give intermediate values of dispersion. Alternately, they may be created over a range
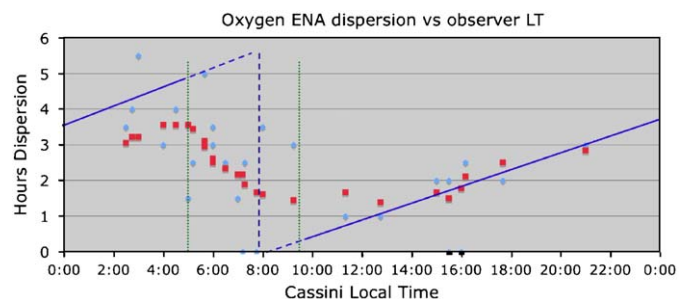

Fig. 4. Light blue points are the measured dispersion (in hours) over the energy range 50–250 keV for each oxygen event analyzed. The red points are a 9 point running boxcar average of the same data. The dark blue lines are a notional fit to the data, with the region between about 0500 and 1000 LT dashed to indicate the jump from maximum to minimum dispersion. The vertical green dotted lines bracket the local times where the dispersion measurement likely represents a mix between zero dispersion and maximum dispersion. The lack of data within two hours of midnight results from INCA's inability to image ENA when the sun is within its field of view.

of local times and so give variable values of dispersion depending on their local time relative to the local time of the spacecraft. In any case there is an unmistakable local time dependence, and it is consistent with the generation of these events in the midnight to dawn quadrant. By generation, or creation, we mean that the ions are heated or accelerated within a confined longitude region and reach some peak intensity, followed by convection and drift as they slowly decay through charge exchange losses, or other loss/cooling mechanisms. The creation or generation time/location is marked at the point where the acceleration/heating ends, and the passive convection/drift begins.

Summarizing these points, we find the phase shifts in ENA peaks apparent in Fig. 2 can be understood as drift dispersion from a single energization event. When we survey oxygen ENAs, it becomes clear to us that the energization processes preferentially occur in the midnight to dawn sector of Saturn's magnetosphere. Next we turn our attention to the high latitude observations of these ENA emissions.

2.2. Relationship of corotating ENA events and auroral processes

At high latitudes the Compton-Getting effect is minimized (the convection vector component along the line of sight becomes smaller with increasing latitude, since the emission, to first order, originates in the equatorial plane) and it is more straightforward for us to follow the brightness maximum in the ENAs in local time.

In the next part of this discussion, we turn to a qualitative description of the MIMI high latitude observations and the possible connections between localized particle acceleration, the SKR period, and auroral emissions. When viewing ring current ENA emission from high latitude, one normally observes asymmetric emission, with the asymmetry rotating about Saturn at roughly the SLS3 rotation period (e.g., Carbary et al., 2008a; Krimigis et al., 2007). This kind of observation does not establish where in local time the particles were initially energized. There are times when during an extended observing period, an initial state with relatively weak ring current ENA emission is followed by an abrupt growth of emission at a well defined local time. That brightening typically peaks an hour to several hours later, while corotating in the same manner as the recurrent events mentioned above. We have surveyed the imaging data set to identify these "new" events, and determine whether there is a repeatable pattern in their locations.

The results of this survey were mixed. We have found instances in which new ENA emissions have appeared at almost any local time. However, among the events where the brightening in both oxygen and hydrogen ENA was pronounced and dispersionless, the new emission usually appeared between midnight and dawn. Sometimes it starts in the pre-midnight quadrant, and sometimes it reaches its peak post-dawn, but it rarely either peaks or initiates between pre-noon and post-dusk.

Although there are many examples of such events, we present only two here, chosen for their clear initiation and growth, for their clear correlations with SKR power enhancements, and in one case a clear association with auroral brightening measured by the Hubble Space Telescope.

The ENA data in Fig. 5 provide the basic features of the first of these events. A period of weak, diffuse emission is interrupted by the sudden appearance of a localized, strong emission in both hydrogen and oxygen ENA (similar to the day 347, 2004 event described in Mitchell et al. 2005a). The emission appears in the same location at different energies and species with peak intensity located well inside the orbit of Titan (outer-most orbit illustrated), and outside the orbit of Rhea; no injection from the tail is observed. The radial position of the onset lies near 15 Rs
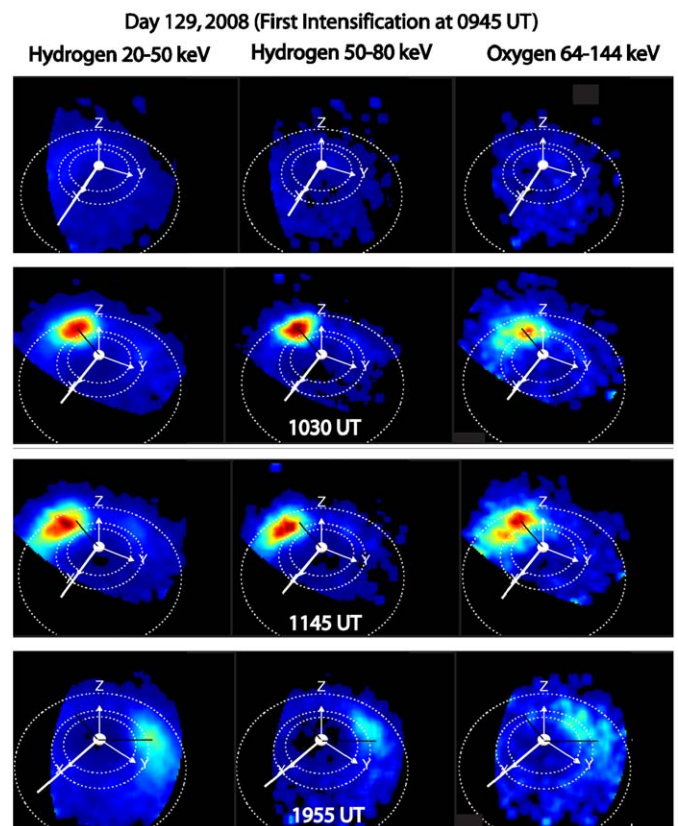

Fig. 5. ENA emission from Saturn's magnetosphere on Day 129, 2008. Heavy white line indicates direction toward sun in every image. The light white arrow points to dusk, and the pink coordinate axes rotate with the planet, indicating the SLS3 system. Light white circles are orbits of Dione (6.5 Rs), Rhea (8.5 Rs, and Titan (20 Rs) for scale and perspective. Each column contains data for the species and energy indicated, and each row is from the time labeled in white in the center column. The images are 1 hour integrations centered at the time indicated. The black diagonal line in the images in the second row is drawn from the center of Saturn to the peak emission in the image. This line is repeated each column, showing the initial enhancement in emission at the same location for each species and energy. The same line is drawn in the third row, to illustrate the rotation of the peak emission over the intervening 1.25 hours. In the bottom row, the line is repeated for reference, and a new line is drawn from the center of Saturn to the peak 20–50 keV H emission (left column). The same line is repeated in the center and right columns, illustrating the additional rotation experienced by the higher energy source ions responsible for the ENA emission in those images.

(assuming the emission can be modeled as coming from the equatorial plane, as has clearly been found when viewing such events from low latitude [Mitchell et al. (2005a), Carbary et al. (2008a), Paranicas et al. (2005)]), and the peak emission remains planetward of 20 Rs throughout the event (emissions at and beyond 20 Rs are sometimes observed, but not in this event; inversion of the ENA images to unfold bias introduced by the radial distribution of the cold neutral gas is beyond the scope of this paper, but the fall-off in intensity of ENA inside ~10–12 Rs can only result from reduced ion intensity, since the gas density decreases monotonically with radial distance). The behavior of this event is quite consistent with the statistical result derived above, in that the event initiation is at the local time identified there, and the oxygen emission is well defined and clearly newly-accelerated. At Earth, the intensifications of oxygen often stand out more clearly than those of hydrogen, and are considered evidence for non-adiabatic acceleration in rapid magnetic field reconfigurations Earthward of and associated with the effects of tail reconnection, such as substorm current sheet acceleration and dipolarization, particularly during geomagnetic storms (Fok et al.,

2006; Mitchell et al., 2005b). In one case a direct association has been made between reconnection and plasmoid formation in Saturn's magnetotail, and one of these ENA sudden enhancements (Hill et al., 2008). This event's primary difference is that it is not viewed from near the equatorial plane, but it is part of an ongoing recurrent sequence of Saturn rotation modulated events, each with a similar sudden increase in ENA intensity in the midnight to dawn quadrant.

Fig. 6 shows the relationship between the ENA emission and SKR emission, as a time series over three days. The SKR enhancements appear at times that are multiples of the 10.8 hour planetary rotation period, with "missing" events late on day 127, early on day 129, and late on day 129. Because spacecraft attitude must be favorable for viewing the magnetosphere, the ENA imaging was not continuous over the three-day period. However imaging was available for several hours around each of the SKR enhancements. While it is difficult in this representation of the data to see the relationship between the onset of the ENA intensification and the onset of the SKR enhancement, it is clear that the peak ENA emission occurs close in time to the peak SKR emission, and the peak ENA emission location is near the dawn meridian in each case.

Fig. 7: To follow the relationship of the development of the ENA enhancement, auroral emission, and the SKR event, Fig. 7 shows the correspondence between ENA emission, SKR power, and the imaged EUV emission in the auroral oval for the event on day 129. Prior to the onset of the enhanced ENA emission at 0900 UT, there was not discernable localized enhancement in the ENA images (Fig. 5, top panel). In panel b) a faint ENA emission appears post-midnight (the X axis of the rotating system, in pink, is aligned with non-midnight at this time). An enhancement in the auroral oval emission also appears at the same longitude. This is just

about the time of the onset of SKR emission, although we have no indication that the SKR is spatially linked with the ENA or the auroral enhancement. In particular, there is a high latitude region post-noon that also brightens at about this time, and develops while moving poleward throughout the observation period. This post-noon feature rotates considerably more slowly than the auroral feature associated with the ENA enhancement, and is likely driven by flow shear near or at the magnetopause as suggested for much of Saturn's auroral emission by Cowley et al. (2004). The auroral emission associated with the ENA enhancement, on the other hand, is quite bright at its equatorward-most limit, which can be seen to extend to $70°$ latitude (mapped images e and f). Clearly the emission is spread over a large range in both latitude and longitude, and appears morphologically much like a storm main phase auroral display on the night side of the Earth.

The ENA emission strength is directly related to the energetic ion intensity in the emission region, and therefore to the contribution to plasma pressure by the energetic ions. Since the region of emission is confined not only in radial distance, but also in local time/longitude, there are pressure gradients both radially and azimuthally implied by the confined emission region. Such azimuthal gradients in pressure will necessarily drive a field-aligned current system, directly analogous to the Region 2 current system associated with the partial ring current at Earth. The resulting field aligned current system may be the system responsible for driving the instability that produces the SKR emission, providing a rather direct causal link between SKR and the bright ENA emission regions in the ring current.

The INCA imager does not have sufficient angular resolution or sensitivity to resolve structure within the emission region. There
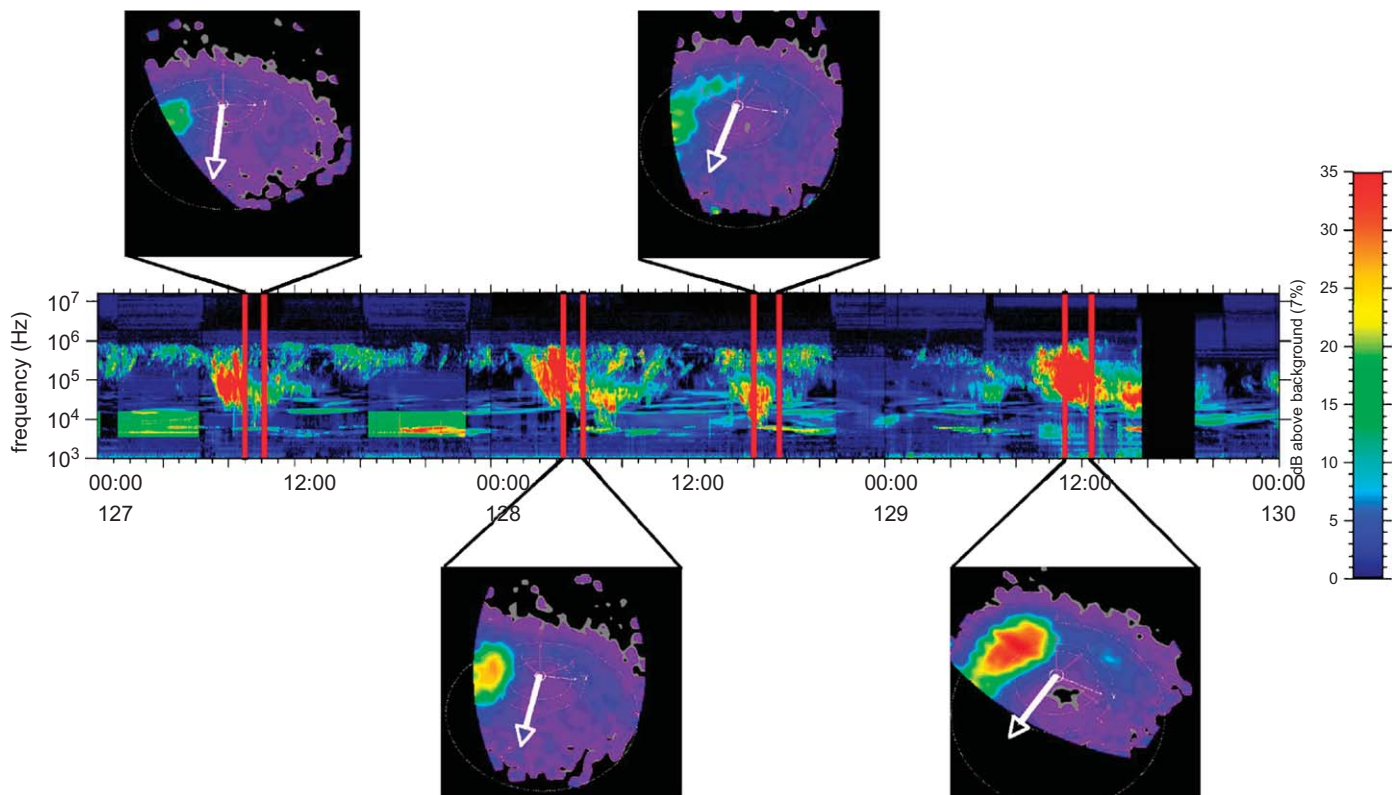

Fig. 6. Days 127 through 129, 2008. Center panel is the Cassini RPWS electric antenna power, with the SKR emission occupying the frequency range between 10^4 and 10^6 Hz. Hydrogen ENA images recorded at the time of the peak of the 20–50 keV emission for each rotation imaged are shown, with registration to the SKR data through the black diagonal lines and red vertical bars. In each case, the peak ENA emission lies very close in time to the peak SKR power, as well as to the lowest frequency excursion of the SKR power. The direction from the center of Saturn toward the sun is indicated by the white arrows in each image.
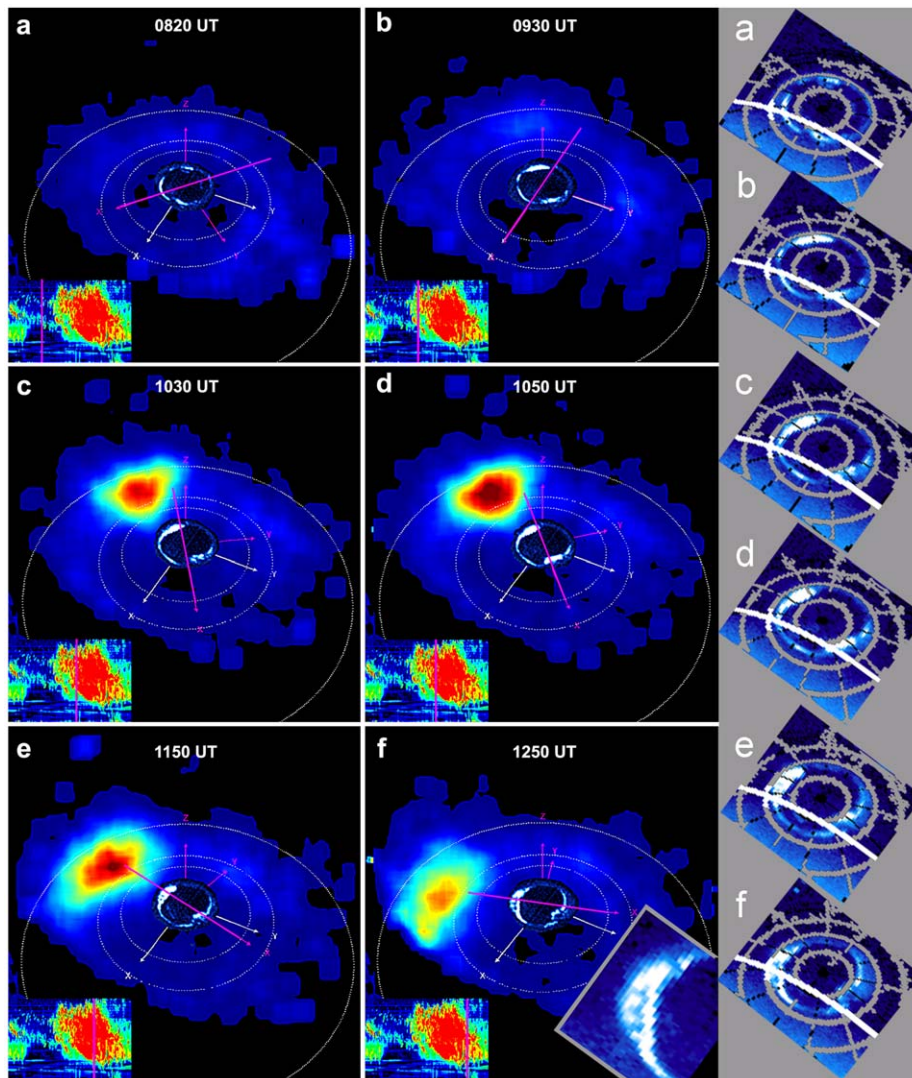
Fig. 7. Six images from the day 129, 2008 sequence. UVIS auroral images scanned over approximately 15 min are superposed, at a larger scale so they can be more easily seen. A pink line lies on top of the X axis of a coordinate system rotating about Saturn's spin axis, at the SLS3 (extrapolated) period. This is for reference, to follow the motion of the ENA enhancement and the bright auroral bulge over time. In the bottom left corner of each frame, the SKR data is reproduced, with a vertical pink line indicating the center time of the hour-long ENA accumulation (time given at top of each frame). To the right, each auroral image is reproduced with a latitude-longitude grid (every 10° of latitude). A white line indicates the terminator, and the 70° latitude line turns to white for a segment where it crosses the terminator. An inset in panel f shows a blow-up of the equatorward bulge at about that time.

may very well be filamentation of the region into smaller hot plasma sub-regions, with sharper gradients and multiple filed aligned current structures linking them to the ionosphere. The auroral emission structure seen in the inset of panel f suggests something like this.

Finally, we present data from the period before and during day 42, 2007 when a solar wind pressure enhancement reached Saturn, triggering enhanced emission in SKR, auroral UV, and energetic neutral atoms. This time period has been presented and discussed in Clarke et al. (2009), where those authors showed that solar wind measurements from 1 AU, propagated to Saturn using an MHD model, predicted the arrival of a strong solar wind pressure enhancement shortly before the SKR and auroral emission enhancements shown in Fig. 8. However, in this presentation, we provide additional data from the ENA images of the ring current, as well as magnetometer data that provide direct evidence for the arrival and magnetospheric response to the solar wind compression event.

Throughout the period shown in Fig. 8, Cassini remained in the northern lobe at about 28 Rs, 58° latitude, and moving from post-dusk to near midnight. Prior to day 42, the lobe magnetic field remains nearly constant, with a weak modulation at the 10.8 hour rotation period of Saturn. This interval was also characterized by very weak SKR emission, low intensity, weak, and structureless ENA ring current emission, and auroral emission below the sensitivity threshold of the HST Wide Field Planetary Camera 2 (which was used when the primary instrument for this campaign, the Advanced Camera for Surveys, went into safe mode). Beginning just after 0300 UT on day 42 (marked by the vertical cyan line) the magnetic field magnitude at Cassini began to increase, quickly at first until 0600 and then more slowly until 1200 UT. This increase is what would be expected as a consequence of a solar wind pressure enhancement and the resultant compression of the magnetosphere. No immediate response is seen in the SKR emission, but the ENA intensity rises with a profile very similar to the magnetic field (although on a log scale). This
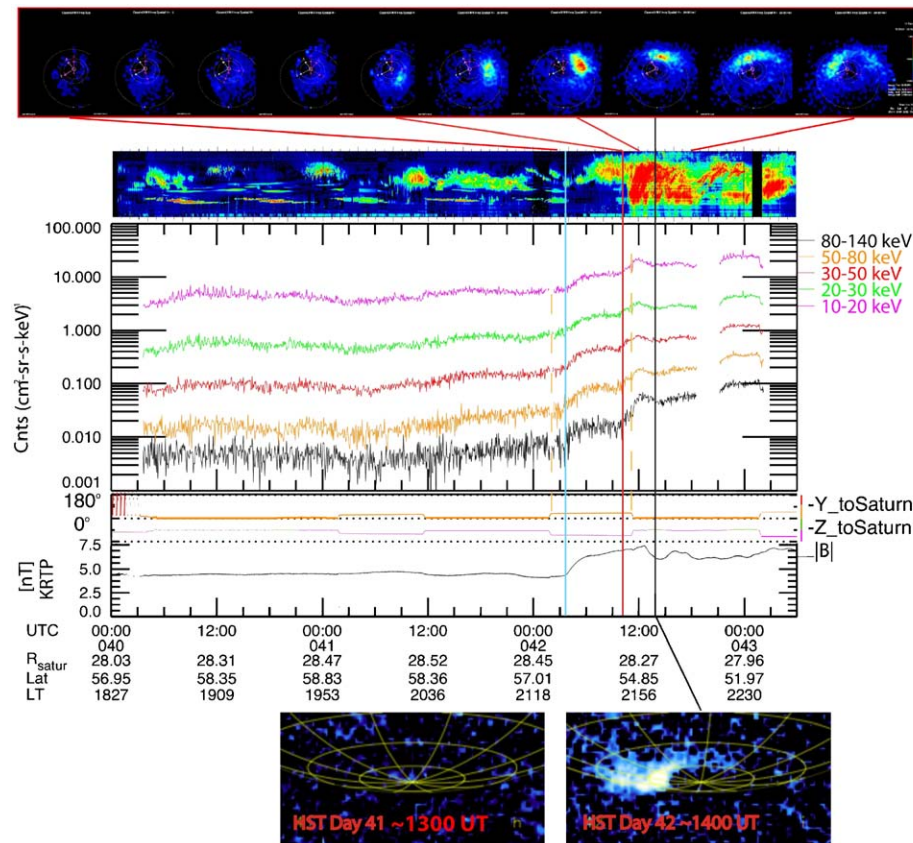
Fig. 8. Solar wind compression event stimulating ENA, SKR, and auroral UV emission at Saturn for days 40–43, 2007. Top panel, sequence of 50–80 keV hydrogen ENA images, with the sun to the upper left, midnight local time to the lower right in each image. Red guide lines indicate their position in the timeline organizing the line plots. Second panel is Saturn kilometric radiation between 1 kHz and 1 MHz. Third panel is ENA emission integrated over the INCA FOV for 5 hydrogen energy channels. The data in the interval between the vertical dashed lines has been moved vertically (all by the same displacement) so that it approximately matches the intensities just prior and just following those times. This was done to compensate for the fact that the spacecraft attitude (characterized by the plots showing the spacecraft −Y and −Z axis angles relative to Saturn body center, fourth and fifth panels) changed in such a way that INCA had only a fraction of the ring current in its FOV for that interval. The sixth panel shows the magnitude of the magnetospheric magnetic field over the 3+ day period shown. The spacecraft, which is at apoapsis during these observations, hardly changes location at all. The bottom images are from the Hubble Space Telescope, and show that on day 41 the auroral oval was quiescent, whereas on day 42, about 1400 UT, bright auroral emission fills the dawn auroral zone.

rise in ENA intensity is simply a global ring current response—the intensity rises throughout the emission region of the ring current, with no local time or radius dominating the rise. At roughly 0700 UT, an enhancement in SKR emission at relatively high frequency appears; whether this is associated with the solar wind pressure enhancement is not clear.

Beginning at about 1030 UT (vertical red line) the ENA emission begins to rise further, this time with a clear local bright emission region very close to local midnight and between 10 and 15 Rs radial distance. This is followed less than an hour later by a strong enhancement in SKR emission, including power extending to much lower frequencies. This kind of SKR response to solar wind compression has been noted before, particularly in Crary et al. (2005) and Mitchell et al. (2005a), and for this particular case in Clarke et al. (2009). Over the next few hours, the ENA intensity increases as the emission region corotates with the general rotation of the magnetospheric plasma. The vertical black line marks the time when the HST WFPC 2 auroral UV image was recorded (corrected for one-way light-travel time); at this time, the ENA emission region was in the late morning local time sector, the same local time where the auroral UV emission appears. The SKR emission remains strong at this time, suggesting well developed field aligned currents, and consistent with the action taking place in the late morning sector where it has been postulated that the most intense SKR emission typically occurs.

The ENA and SKR emission both remain elevated for the remainder of day 42 and into day 43, after which the spacecraft attitude changes and INCA can no longer image the ring current. After ~1245 UT, the magnetic field strength decreases. Whether this is related to an unloading of pressure from the magnetotail (e.g. through plasmoid release), or a reflection of pressure variations in the solar wind, we have no way of knowing.

3. Discussion

Our analysis of ENA images reveals another feature for the organization of periodicities in Saturn's magnetosphere. This is that a class of localized ring current enhancements, wherein the energetic ion intensities (and particularly including oxygen intensities) are enhanced by about an order of magnitude above the adjacent ring current regions, have a preferred local time for initiation. Based both on the dispersion analysis presented at the beginning of this paper, and on high latitude imaging such as that shown in the later sections, a picture emerges that has acceleration events beginning preferentially near local midnight, and growing in intensity and volume over the next several hours as they corotate through dawn into the late morning local time sector, where they begin to decay. The particles that are energized during the event growth phase then continue to partially corotate,

drift azimuthally by gradient and curvature drifts, and lose numbers and energy both through charge exchange losses as well as escape through the magnetopause as they rotate through noon.

After one circuit around the magnetosphere many of the original particles have been lost although enough remain that the event can sometimes still be detected remotely by ENA imaging as a coherent (though energy-dispersed) hot plasma population. Because of its higher cross section for charge exchange with the cold equatorial gas population produced by Enceladus and distributed throughout the magnetosphere, oxygen is lost more quickly than hydrogen. Thus as the acceleration of a new population takes place on each new rotation of the magneto-sphere, the oxygen dispersion signature remains essentially stationary, so that the same dispersion characteristic is seen as a function of observer local time rotation after rotation, and from one epoch to another. Hydrogen, with its longer lifetime against charge exchange, does not produce such a simple pattern, as older more dispersed events mix with newer, less dispersed events.

This behavior can be viewed as a resulting from a requirement for both a preferred local time at which an instability may initiate and grow (roughly midnight to the dawn meridian), and a preferred longitude or range of longitudes locked to the rotating magnetosphere/ionosphere system that favors the growth of an instability, which in combination triggers the instability once per rotation. So while this analysis has not provided us with the information as to what makes a particular longitude (or long-itudinal hemisphere) favorable for the instability, it has shown us where in local time the asymmetry is impressed, at least for energetic particles in the ring current.

The analysis in Section 2.2 provides interesting associations between the initiation and location of ring current energetic particle enhancements, and the generation of both Saturn kilometric radiation and auroral UV emissions. We have chosen events for which the initial state of the ring current is fairly uncomplicated, and for which there is a robust and relatively simple enhancement in ring current ENA emission. In the first of the two cases shown, the ENA and SKR enhancements belong to a series of recurrent events that had been going on for several days. The particular recurrence on day 129 was one of the more prominent of the series, and the orbital position and observation schedule were well suited to cover the phenomenology. In the second case, the event was associated with a magnetospheric compression by the solar wind, and does not appear to be synchronous with the magnetospheric rotational periodicity. So while the two events are superficially similar, the first belongs to the same class of events for which the dispersion analysis in Section 2.1 was conducted, while the second belongs to the class of events clearly initiated by the impingement of a solar wind pressure pulse. Because the ENA enhancements in these events are much stronger than what immediately precedes them, the potential to be confused by possibly competing contributions to the ENA images is reduced. Likewise, the time histories of the other remote sensing measurements (and in situ, in the case of the magnetic field) are also simple, so that the phenomenology associated with the ENA enhancements may be more directly associated with those enhancements than would be possible under more complex, confusing conditions.

In the first (for which a rotation-modulated event had been in progress for several Saturn rotations and we have good contin-uous viewing of the ring current with INCA from high latitude) the emission enhancement is well localized in radius and azimuth, and the ENA emission is strong and well defined in both hydrogen and oxygen. We show that the azimuthal propagation of the particles, viewed directly from high northern latitude, exhibits the same energy dependent motion that we capitalized on for the statistical dispersion analysis in Section 2.1. So this event appears to be similar in all important respects to the events through which we established the midnight to dawn quadrant as the unique initiation site for the recurrent corotating ring current enhance-ments. We then showed (Fig. 6) that these events were well correlated in time with the series of SKR emission enhancements measured over the same period.

Looking in closer detail at the ENA and SKR emissions on the Day 129, 2008 manifestation of the recurrent event shown in Fig. 6, we found (Fig. 7) that the growth in the intensity of the localized ENA emission in the newly formed corotating region appeared to be closely correlated both with the longitude and brightness of a corotating auroral bulge, as well as with the growth of both the total power and the lower frequency extent of the SKR emission. The observed SKR power is a very complex quantity, dependent on the details of the geometry of the emission cone, the latitude, altitude and local time of the emission region, and the position of the spacecraft relative to the emission region (e.g., Lamy et al., 2008). It is beyond the scope of this paper to attempt to unravel all of those effects, as it is also beyond the scope of this paper to attempt to model the ring current structure and derive field aligned currents from it. However, the associa-tions appear to be good, and there is qualitative reason to suppose that it may be causal, especially in the case of the auroral emission. Azimuthal asymmetries in ring current pressure (e.g., energetic ion intensity) result in current divergence that must be closed via field aligned currents (as in the case of the storm-time partial ring current at Earth). Thus, the corotating energetic ion intensity enhancements in the ring current must be flanked on both their leading and trailing edges by field aligned current structures that map from the ring current into the ionosphere. Unresolved longitudinal substructure within the ring current enhancement might result in a series of smaller scale azimuthal gradients with a subsequent series of pairs of filed aligned currents linked with the longitudinal structure apparent in the auroral bulge. How those currents close in the ionosphere is not important for making the association with SKR—the fact that we have a corotating field aligned current generator, whose strength as measured by the intensity of both the ENA and auroral emission is correlated with the current driven SKR emission suggests that they may be linked. In any case, the SKR emission requires some kind of rotation modulated field aligned current structure, and the asymmetric ring current is a plausible source for that current. Such a rotating current system could also be responsible for the oscillation of Saturn's auroral oval with amplitude $\sim 1°-2°$ and period consistent with the concurrent magnetometer and SKR periods, as observed by Nichols et al. (2008). For example, these authors showed that the magnetic perturbations associated with the non-axisymmetric convection model of Goldreich and Farmer (2007) may be expected to shift the auroral oval by $\sim 1.5°$.

The details of the coupling of the field aligned currents with the ionosphere may have other important implications. Since the ionospheric conductance is different in the south than in the north during this epoch of southern summer, the field aligned currents driven by the ring current pressure gradients and flowing into and out of each hemisphere may not be of equal magnitudes. A rotating field aligned current system consistent with this scenario has recently been derived from high latitude magnetic perturbations by Provan et al. (2009). This inequality can be viewed as a symmetric term (equal currents into each hemi-sphere) superposed with currents flowing from one hemisphere to the other. The latter has been suggested to explain some of the rotating magnetic perturbations seen in the middle magneto-sphere (e.g., Southwood and Kivelson, 2007).

The peak SKR intensity occurs at about the time that the ENA emission reaches its peak intensity, which is also when the ENA enhancement reaches late morning local time. It has long been claimed that the most probable local time of SKR emission was late morning [e.g., Cecconi and Zarka (2005)]. The growth and decay of ENA events as they progress from midnight through noon is consistent with that scenario, in that the peak ring current enhancement seems typically to occur near, or just past dawn, where it would be driving field aligned currents in the same general region required to explain the SKR phenomenology. This in itself does not prove causality, but the association is clear.

Lastly, we presented an event unique in several respects, not the least of which was that there was HST auroral imaging available. This event has already been discussed by Clarke et al. (2009), who show that the auroral emission on the dawn side of the oval is both well correlated with a strong enhancement in SKR power, and also with a solar wind pressure enhancement associated with a corotating interaction region, and preceded by a long solar wind rarefaction region as propagated from 1 AU using an MHD simulation. Based on the understanding gained by Crary et al (2005), Jackman et al. (2005), and others, the preceding rarefaction region should be associated with quiet magnetospheric and auroral conditions, with the likelihood of a background rotation modulated low level of activity, but relatively weak SKR emission. This was indeed observed, as demonstrated in the figure by weak, steady ENA emission, weak SKR emission exhibiting some rotation modulation, and nearly constant magnetic field strength with a slight modulation at the rotation period. At about the time identified in Clarke et al. (2009) based on propagated measurements from 1 AU (remarkably close, given the estimated errors for such propagation), the magnetic field strength began to rise, consistent with the arrival of a solar wind compression region at the planet. The locally measured lobe magnetic field strength rises by a factor of about 1.4 over about 2–3 hours, implying a change in pressure by about a factor of 2, then more slowly for about 6 more hours. The profile of the intensity of ENA emission is similar, again consistent with a compression of the magnetosphere–as the lobe pressure rises by a factor of 2, the particles in the ring current are compressed and adiabatically accelerated, increasing their intensity at a given energy by a similar factor of about 2 such that the ring current particle pressure balances the increased lobe pressure. Such an effect is commonly seen at Earth as well (e.g., Lee et al., 2007). Up to this point, there is little evidence for more than a passive response by the magnetosphere to the increase in solar wind pressure. However, beginning at about 10:30 UT, a bright, localized patch of hydrogen ENA emission appears near midnight and subsequently increases in both intensity and area (volume) as the region rotates about Saturn under the influence of the corotation electric field. As this ring current region intensifies and rotates to the dawn meridian, the SKR emission abruptly intensifies, actually leading at low frequencies (unlike the event discussed in Figs. 6 and 7). This strong SKR emission enhancement comes about 4 hours after a weaker enhancement whose timing is about right to be one of the weak events modulated at the rotation period. This makes the bright enhancement late, and possibly independent of the mechanism responsible for the rotational modulation. About two hours later, the only HST image for that day is made, and the bright emission appears on the dawn side. The radiated power of this emission is about 23 GW, the brightest emission seen during the 2007 HST Saturn campaign (for which the average power was about 10 GW). It is at least plausible that a similar field aligned current structure, driven by azimuthal ring current pressure gradients as discussed above, is responsible for both the enhanced SKR emission and the auroral brightening, especially given the alignment in local time of the latter with the

ring current enhancement. Again, we cannot prove a direct causal relationship, but the circumstantial evidence for a connection is, we believe, compelling. Another possibility is that precipitation of energetic particles from the hot ENA-emitting plasma causes the bright auroral emission. Although we have not investigated this possibility in any detail, we do not favor this interpretation. Regarding ion precipitation, we have never seen an ENA signature of bright precipitation emission at Saturn, a signature seen very clearly, even dominantly in ENA emissions at Earth during magnetic storms. The ratio in magnetic field strength between the ring current at 12–15 Rs ($\sim$5–10 nT) and the field strength at the surface ($\sim$4000 nT) corresponds to a loss cone of the order of $0.1°$, so even if there were strong ion scattering, very little of the equatorial particle flux can reach the atmosphere without a parallel potential to move more particles into the loss cone. Furthermore, ions are very inefficient in producing auroral emissions. We have no direct means of determining whether strong electron scattering is occurring in these events, but the frequent occurrence of strongly peaked bidirectional field aligned auroral electrons (Mitchell et al., 2009) suggest that electron scattering is usually minimal.

This possible association of auroral emission and dawn side ENA events may also help explain the tendency for bright auroral emissions to favor the dawn meridian even during quiet times, as described in Gérard et al. (2006). As established above, the pattern that repeats itself during undisturbed times is often a rotation modulated state, with ring current acceleration events initiated near midnight and corotating while growing through dawn toward noon. If these ring current asymmetric pressure enhancements drive field aligned currents (again analogous to the partial ring current, or the substorm current wedge at Earth) then it might be expected that the brightest auroral emissions during such externally quiescent periods would appear in the rotation cycle where the ring current pressure enhancement reaches its peak, and that is close to the dawn meridian. This might even be expected for non-rotationally modulated relatively quiet time, if the observed dawn emission is driven from the ring current, and the non-modulated ring current also has a tendency to peak in its intensity near dawn. This has not been established, and is simply mentioned here as a possibility for future investigation.

If the ring current enhancements are directly causally linked with auroral emissions and SKR, then the implication is that at least some fraction of Saturn's auroral emission is internally driven, and not directly related to the solar wind interaction (although as in the last event, it may be indirectly enhanced by that interaction). Past publications that concluded that the Saturn aurora must be driven exclusively by solar wind shear reached that conclusion based on calculation of field aligned current strength in the inner and middle magnetosphere assuming a cylindrically symmetric system with frictional and pick-up loading drag forces (e.g., Cowley et al., 2004). Their conclusion was that in the middle magnetosphere, the field aligned current structure implied was easily supplied by the ambient plasma, without the need for field aligned potentials to supply the required current, while in the vicinity of the open-closed boundary, potentials of the order of 10 kV are required. However, the observations here suggest a different, asymmetric mechanism for generating field aligned currents (namely ring current pressure asymmetry), which may in fact generate sufficiently high currents that field aligned acceleration is required to supply the current carriers, resulting in recurrent bright auroral arcs that favor the dawn meridian as well as late morning local time. (Radioti et al., 2009 have also made associations between in situ energetic particle events and Saturn auroral emissions, but these are of much smaller scale than the event discussed here, and are attributed to direct energetic particle precipitation rather than to

field aligned current structures.) The possibility also remains that auroral displays associated with ring current enhancements are produced by enhanced particle precipitation from those enhancements, although we do not favor that interpretation for reasons stated above.

The location of the initiation of ENA brightening near midnight also suggests that these events are associated with current sheet reconnection and subsequent plasmoid release down the tail. Whether the imaged emission is in a reconnection region, or planetward of such a region, the occurrence once per rotation is in agreement with the observation of rotation period events in the tail plasma sheet (Burch et al., 2008). And in at least one case, a direct association has been made between the observation of a plasmoid passage in the magnetotail and the occurrence of an ENA event with just the appropriate location and timing to have been a remote observation of the plasmoid release (Hill et al., 2008). The midnight location for onset is a natural one for reconnection, as the night side ring current and plasma sheet are far thinner than they are on the dayside (Sergis et al., 2007).

This mechanism is different from that suggested by Sittler et al. (2006) who suggested that auroral emission might be caused by enhanced flux tube interchange triggered by solar wind compression. However, the mechanism suggested by Sittler et al. (2006) might supplement the process we are invoking, in the sense that reconnection on closed field lines ("Vasyliunas-cycle" reconnection; Vasyliunas, 1983) might empty cold plasma from a particular longitudinal segment in the outer magnetosphere beyond 15 Rs, steepening the pressure gradient near 15 Rs in that longitudinal sector. With a steeper radial gradient, flux tube interchange would be more favored (the empty flux tubes would be more buoyant) and might account for the spreading of the ENA emission inward from 15 Rs to less than 8 Rs, as the low density, hot flux tubes move planetward and their particles are adiabatically heated.

The scenario we are postulating is perhaps more directly comparable to that suggested by Cowley et al. (2005), wherein it was asserted that the auroral forms observed by the HST were naturally explained by reconnection near midnight, with subsequent corotation of the planetward side of the reconnection accelerated plasma and field reorganization through dawn, then noon and dusk. That study (like the Sittler et al., 2006 study) particularly addressed solar wind compression driven activity, as for example during the January 2004 period studied in Crary et al. (2005). One primary difference we are suggesting is that tail reconnection continues to occur even during periods undisturbed by solar wind pressure variations, and on a very regular basis (modulated by Saturn's rotation as coupled through the ionosphere to the magnetosphere). We suggest that this is "Vasyliunas-cycle" reconnection on closed plasma sheet field, internally driven by the need to unload cold plasma from stretched field lines, and not necessarily involving lobe field reconnection.

This recurrent, internally driven reconnection, when taken together with the mechanism we are suggesting for linking it to the dawn aurora, provides a natural explanation for the spontaneous dawn auroral brightening without apparent external trigger, noted originally by Gérard et al. (2006).

4. Conclusions

We show that:

(1) Recurrent ring current oxygen intensity enhancements begin near midnight and increase in intensity and area as they rotate through the dawn meridian toward noon.
(2) There is a close temporal association between recurrent ring current enhancements and recurrent SKR enhancements.

(3) In the single manifestation of this recurring phenomenon for which continuous UV auroral imaging was available, bright corotating auroral emissions distributed in latitude from 70° to 80° tracked the ring current ion enhancement as it moved in local time from post midnight to late morning.
(4) A strong correlation exists between a solar wind pressure pulse resulting in magnetospheric compression and a ring current event, a sudden SKR power increase, and dawn side auroral brightening.

We suggest a link between the asymmetric ring current enhancements and a rotating field aligned current system that drives both SKR enhancements and auroral displays. Such a relationship is implied for both recurrent events with the Saturn rotation period and solar wind pressure induced events. Based on this work as well as the close resemblance of the events studied here with previous analyses (e.g., Hill et al., 2008; Mitchell et al., 2005a, b), we suggest that these recurrent events are caused by recurrent reconfiguration of the thin night-side current sheet in the 15–20 Rs region, probably associated with "Vasyliunas-cycle" reconnection and plasmoid release in the tail initiated relatively close to Saturn. The energy in such events presumably derives from Saturn's rotation, in combination with the mass loading of the cold plasma produced from Enceladus' extended gas cloud.

Appendix A. Supplementary materials

Supplementary data associated with this article can be found in the online version at doi:10.1016/j.pss.2009.04.002

References

Brandt, P.C., Paranicas, C.P., Carbary, J.F., Mitchell, D.G., Mauk, B.H., Krimigis, S.M., 2008. Understanding the global evolution of Saturn's ring current. Geophys. Res. Lett. 35, L17101.
Bunce, E.J., Arridge, C.S., Cowley, S.W.H., Dougherty, M.K., 2008. Magnetic field structure of Saturn's dayside magnetosphere and its mapping to the ionosphere: Results from ring current modeling. J. Geophys. Res. 113, A02207.
Burch, J.L., Goldstein, J., Mokashi, P., Lewis, W.S., Paty, C., Young, D.T., Coates, A.J., Dougherty, M.K., André, N., 2008. On the cause of Saturn's plasma periodicity. Geophys. Res. Lett. 35, L14105.
Carbary, J.F., Mitchell, D.G., Krimigis, S.M., Krupp, N., 2007a. Electron periodicities in Saturn's outer magnetosphere. J. Geophys. Res. 112, A03206.
Carbary, J.F., Mitchell, D.G., Krimigis, S.M., Hamilton, D.C., Krupp, N., 2007b. Charged particle periodicities in Saturn's outer magnetosphere. J.Geophys. Res. 112, A06246.
Carbary, J.F., Mitchell, D.G., Brandt, P., Paranicas, C., Krimigis, S.M., 2008a. ENA periodicities at Saturn. Geophys. Res. Lett. 35, L07102.
Carbary, J.F., Mitchell, D.G., Brandt, P., Roelof, E.C., Krimigis, S.M., 2008b. Statistical morphology of ENA emissions at Saturn. J. Geophys. Res. 113, A05210.

Cecconi, B., Zarka, P., 2005. Model of a variable radio period for Saturn. J. Geophys. Res. 110, A12203.

Clarke, J.T., Nichols, J., Gérard, J.-C., Grodent, D., Hansen, K.C., Kurth, W., Gladstone, G.R., Duval, J., Wannawichian, S., Bunce, E., Cowley, S.W.H., Crary, F., Dougherty, M., Lamy, L., Mitchell, D., Pryor, W., Retherford, K., Stallard, T., Zieger, B., Zarka, P., Cecconi, B., 2009. Response of Jupiter's and Saturn's auroral activity to the solar wind. J. Geophys. Res. 114, A05210, doi:10.1029/2008JA013694.

Cowley, S.W.H., Bunce, E.J., O'Rourke, J.M., 2004. A simple quantitative model of plasma flows and currents in Saturn's polar ionosphere. J. Geophys. Res. 109, A05212.

Cowley, S.W.H., Badman, S.V., Bunce, E.J., Clarke, J.T., Gérard, J.-C., Grodent, D., Jackman, C.M., Milan, S.E., Yeoman, T.K., 2005. Reconnection in a rotation-dominated magnetosphere and its relation to Saturn's auroral dynamics. J. Geophys. Res. 110, A02201.

Crary, F.J., Clarke, J.T., Dougherty, M.K., Hanlon, P.G., Hansen, K.C., Steinberg, J.T., Barraclough, B.L., Coates, A.J., Gérard, J.-C., Grodent, D., Kurth, W.S., Mitchell, D.G., Rymer, A.M., Young, D.T., 2005. Solar wind dynamic pressure and electric field as the main factors controlling Saturn's aurorae. Nature 433, 720–722 J. Geophys. Res., 110, A10212.

Fok, M.-C., Moore, T.E., Brandt, P.C., Delcourt, D.C., Slinker, S.P., Fedder, J.A., 2006. Impulsive enhancements of oxygen ions during substorms. J. Geophys. Res. 111, A10222, doi:10.1029/2006JA011839.

Gérard, J.-C., Grodent, D., Cowley, S.W.H., Mitchell, D.G., Kurth, W.S., Clarke, J.T., Bunce, E.J., Nichols, J.D., Dougherty, M.K., Crary, F.J., Coates, A.J., 2006. Saturn's auroral morphology and activity during quiet magnetospheric conditions. J. Geophys. Res. 111, A12210.

Giampieri, G., Dougherty, M.K., Smith, E.J., Russell, C.T., 2006. A regular period for Saturn's magnetic field that may track its internal rotation. Nature 441, 62–64.

Goldreich, P., Farmer, A.J., 2007. Spontaneous axisymmetry breaking of the external magnetic field at Saturn. J. Geophys. Res. 112, A05225.

Hill, T.W., Thomsen, M.F., Henderson, M.G., Tokar, R.L., Coates, A.J., McAndrews, H.J., Lewis, G.R., Mitchell, D.G., Jackman, C.M., Russell, C.T., Dougherty, M.K., Crary, F.J., Young, D.T., 2008. Plasmoids in Saturn's magnetotail. J. Geophys. Res. 113, A01214.

Jackman, C.M., Achilleos, N., Bunce, E.J., Cecconi, B., Clarke, J.T., Cowley, S.W.H., Kurth, W.S., Zarka, P., 2005. Interplanetary conditions and magnetospheric dynamics during the Cassini orbit insertion fly-through of Saturn's magnetosphere. J. Geophys. Res. 110, A10212.

Jurac, S., Richardson, J.D., 2005. A self-consistent model of plasma and neutrals at Saturn: neutral cloud morphology. J. Geophys. Res. 110, A09220.

Kane, M., Mitchell, D.G., Carbary, J.F., Krimigis, S.M., Crary, F.J., 2008. Plasma convection in Saturn's outer magnetosphere determined from ions detected by the Cassini INCA experiment. Geophys. Res. Lett. 35, L04102.

Krimigis, S.M., Mitchell, D.G., Hamilton, D.C., Livi, S., Dandouras, J., Jaskulek, S., Armstrong, T.P., Boldt, J.D., Cheng, A.F., Gloeckler, G., Hayes, J.R., Hsieh, K.C., Ip, W.-H., Keath, E.P., Kirsch, E., Krupp, N., Lanzerotti, L.J., Lundgren, R., Mauk, B.H., McEntire, R.W., Roelof, E.C., Schlemm, C.E., Tossman, B.E., Wilken, B., Williams, D.J., 2004. Magnetospheric Imaging Instrument (MIMI) on the Cassini Mission to Saturn/Titan. Space Sci. Rev. 114, 233–329.

Krimigis, S.M., Mitchell, D.G., Hamilton, D.C., Krupp, N., Livi, S., Roelof, E.C., Dandouras, J., Armstrong, T.P., Mauk, B.H., Paranicas, C., Brandt, P.C., Bolton, S., Cheng, A.F., Choo, T., Gloeckler, G., Hayes, J., Hsieh, K.C., Ip, W.-H., Jaskulek, S., Keath, E.P., Kirsch, E., Kusterer, M., Lagg, A., Lanzerotti, L.J., LaVallee, D., Manweiler, J., McEntire, R.W., Rasmuss, W., Saur, J., Turner, F.S., Williams, D.J., Woch, J., 2005. Dynamics of Saturn's magnetosphere from MIMI during Cassini's orbital insertion. Science 307, 1270–1273.

Krimigis, S.M., Sergis, N., Mitchell, D.G., Hamilton, D.C., Krupp, N., 2007. A dynamic, rotating ring current around Saturn. Nature 450, 1050–1053.

Kurth, W.S., Averkamp, T.F., Gurnett, D.A., Groene, J.B., Lecacheux, A., 2008. An update to a Saturnian longitude system based on kilometric radio emissions. J. Geophys. Res. 113, A05222.

Lamy, L., Zarka, P., Cecconi, B., Prange', R., Kurth, W.S., Gurnett, D.A., 2008. Saturn kilometric radiation: Average and statistical properties. J. Geophys. Res. 113, A07201.

Lee, D.-Y., Ohtani, S., Brandt, P.C., Lyons, L.R., 2007. Energetic neutral atom response to solar wind dynamic pressure enhancements. J. Geophys. Res. 112, A09210.

Mauk, B.A., Saur, J., Mitchell, D.G., Roelof, E.C., Brandt, P.C., Armstrong, T.P., Hamilton, D.C., Krimigis, S.M., Krupp, N., Livi, S.A., Manweiler, J.W., Paranicas, C.P., 2005. Energetic particle injections in Saturn's magnetosphere. Geophys. Res. Lett. 32, L14S05.

Mitchell, D.G., Brandt, P.C., Roelof, E.C., Dandouras, J., Krimigis, S.M., Mauk, B.H., Paranicas, C.P., Krupp, N., Hamilton, D.C., Kurth, W.S., Zarka, P., Dougherty, M.K., Bunce, E.J., Shemansky, D.E., 2005a. Energetic ion acceleration in Saturn's magnetotail: Substorms on Saturn? Geophys. Res. Lett. 32, 2005GL022647.

Mitchell, D.G., Brandt, P.C., Mende, S.B., 2005b. Oxygen in the ring current during major storms. Advances in Space Research 36, 1758–1761 {2005AdSpR. 36.1758M}.

Mitchell, D.G., Kurth, W.S., Hospodarsky, G.B., Krupp, N., Saur, J., Mauk, B.H., Carbary, J.F., Krimigis, S.M., Dougherty, M.K., Hamilton, D.C., 2009. Ion conics and electron beams associated with auroral processes on Saturn. J. Geophys. Res. 29 (114), XXXXXX.

Nichols, J.D., Clarke, J.T., Cowley, S.W.H., Duval, J., Farmer, A.J., Gérard, J.-C., Grodent, D., Wannawichian, S., 2008. Oscillation of Saturn's southern auroral oval. J. Geophys. Res. 113, A11205.

Paranicas, C.P., Mitchell, D.G., Roelof, E.C., Brandt, P.C., Williams, D.J., Krimigis, S.M., Mauk, B.H., 2005. Periodic intensity variations in global ENA images of Saturn. Geophys. Res. Lett. 32, 2005GL023656.

Paranicas, C., Mitchell, D.G., Roelof, E.C., Mauk, B.H., Krimigis, S.M., Brandt, P.C., Kusterer, M.B., Turner, F.S., Vandegriff, J.D., Krupp, N., 2007. Energetic electrons injected into Saturn's neutral gas cloud. Geophys. Res., Lett. 34, L02109.

Provan, G., Andrews, D.J., Arridge, C.S., Cowley, S.W.H., Milan, S.E., Dougherty, M.K., Wright, D.M., 2009. Polarization and phase of planetary-period magnetic field oscillations on high latitude field lines in Saturn,s magnetosphere. J. Geophys. Res. 114, A02225.

Radioti, A., Grodent, D., Gérard, J.-C., Roussos, E., Paranicas, C., Bonfond, B., Mitchell, D.G., Krupp, N., Krimigis, S., Clarke, J.T., 2009. Transient auroral features at Saturn: signatures of energetic particle injections in the magnetosphere, in press. J. Geophys. Res.

Sergis, N., Krimigis, S.M., Mitchell, D.G., Hamilton, D.C., Krupp, N., Mauk, B.M., Roelof, E.C., Dougherty, M., 2007. Ring current at Saturn: Energetic particle pressure in Saturn's equatorial magnetosphere measured with Cassini/MIMI. Geophys. Res. Lett. 34, L09102.

Shemansky, D.E., Hall, D.T., 1992. The distribution of atomic hydrogen in the magnetosphere of Saturn. J. Geophys. Res. 97, 4143–4161.

Sittler Jr., E.C., Blanc, M.F., Richardson, J.D., 2006. Proposed model for Saturn's auroral response to the solar wind: Centrifugal instability model. J. Geophys. Res. 111, A06208.

Southwood, D.J., Kivelson, M.G., 2007. Saturnian magnetospheric dynamics: Elucidation of a camshaft model. J. Geophys. Res. 112, A12222.

Vasyliunas, V.M., 1983. Plasma distribution and flow. In: Dessler, A.J. (Ed.), Physics of the Jovian Magnetosphere. Cambridge Univ. Press, New York, p. 395.